Growth of long-range correlations in a transition between heat conduction and convection

Tadashi Watanabe, Hideo Kaburaki, Masahiko Machida, and Mitsuo Yokokawa
Computing and Information Systems Center, Japan Atomic Energy Research Institute, Tokai-mura, Naka-gun, Ibaraki-ken, 319-11, Japan
(Received 31 May 1994; revised manuscript received 17 March 1995)

The transition between heat conduction and convection in the two-dimensional Rayleigh-Bénard system is simulated using the direct simulation Monte Carlo method. Long-range correlations of temperature fluctuations are found to grow in the transition.

PACS number(s): 47.20.Bp, 47.27.Te, 05.70.Ln, 05.40.+j

I. INTRODUCTION

The Rayleigh-Bénard (RB) system, in which a fluid is contained between two horizontal parallel walls and the bottom wall is kept at a higher temperature than the top wall, is one of the representative nonequilibrium hydrodynamic systems. In the RB system, a heat conduction state is established when the temperature difference between the top and bottom walls is smaller than a critical value, while convection rolls appear when the temperature difference exceeds the critical value. A transition between conduction and convection is known as the RB instability.

Convection in the RB system has been studied by many researchers experimentally [1] and numerically [2]. In recent years, RB convection has been studied at the molecular level using the molecular dynamics (MD) method and the direct simulation Monte Carlo (DSMC) method in order to study the microscopic origin of the macroscopic flow phenomena. The convection rolls were simulated using the MD method [3], and the field variables were compared with the results by the hydrodynamic calculations [4]. RB convection was also simulated using the DSMC method [5], and the results were compared with the numerical solution of the Navier-Stokes equation [6]. Although convection rolls were observed, the transition between conduction and convection was not discussed in these MD and DSMC simulations. The transition in the RB system was shown by Watanabe, Kaburaki, and Yokokawa using the DSMC method [7]. The bifurcation of temperature distribution between conduction and convection was observed at around the hydrodynamic critical Rayleigh number. It was pointed out that the microscopic structures in macroscopic flow transitions and instabilities could be studied using the DSMC method.

In order to study fluctuations in nonequilbrium thermodynamic systems, spatial correlation functions of field variables have been studied. Nicolis and Mansour derived the correlation function from a multivariate master equation, and applied it to a problem of heat conduction in a fluid submitted to a temperature gradient [8]. The spatial correlation function in the direction of the temperature gradient was shown to be long ranged in the nonequilibrium steady state. Long-range spatial correlations were observed in heat conduction using the MD [9] and DSMC methods [10]. It was shown in these theoretical and numerical studies that the nonequilibrium part of the temperature correlation function was proportional to the square of the temperature gradient. Garcia *et al.* [11] and Mansour *et al.* [12] obtained the correlation functions by solving the linearized fluctuating hydrodynamic equations. The calculated results were in good agreement with the DSMC results, and the fluctuating hydrodynamics was suggested to provide a way to study hydrodynamic instabilities [12]. Thermodynamic fluctuations in heat conduction were studied well in terms of correlation functions in the direction of the temperature gradient, but neither the nonequilibrium system with an external field such as gravity nor the macroscopic flow instability was studied.

The correlation functions in a thin layer of a nematic liquid crystal have been observed experimentally by Rehberg *et al.* [13] The experiments were conducted under a condition below the onset of electroconvection. Horizontal correlation functions in a large aspect-ratio sample were measured, and the fluctuations were shown to be described by a stochastic mean-field model. It was mentioned, however, that the electroconvection in nematics was not expected to be in the same universality class as RB convection.

In this paper, the DSMC method of Bird [14] is applied to simulate the RB instability for studying the microscopic structure in the macroscopic flow instability. The fluctuations of temperatures in the transition between heat conduction and convection are discussed in terms of spatial correlations in vertical direction.

II. SIMULATION OF THE RAYLEIGH-BÉNARD SYSTEM

The RB conduction-convection system is simulated using the DSMC method, which is one of the most widely used numerical techniques for simulating rarefied gas flows with incorporating atomistic details. This technique was developed by Bird [14] and has been applied to various types of flow problems. In this method, a large number of molecules in a real gas are simulated by a smaller number of representative particles. The trajectories of these particles are traced in a short time interval

by decoupling interparticle collisions and taking interactions with boundaries into account. Interparticle collisions take place on a probabilistic basis in a collision cell. Macroscopic quantities are obtained by sampling particle properties in a sampling cell, which is generally larger than the collision cell.

In the present simulation of the RB system, the computational region is a two-dimensional rectangle, which is 11.3 mm in width and 5.6 mm in height, with an aspect ratio of 2.016. Three-dimensional calculations are performed for interparticle collisions, and each particle has three velocity components in the Cartesian coordinate, but only two directions are considered for the trajectories of particles. The computational region is surrounded by flat walls and filled with hard sphere particles with a diameter of 3.7×10^{-10} m and a mass of 4.8×10^{-26} kg. The Prandtl number is 0.67. The initial temperature and pressure are assumed to be 80 K and 20 Pa, respectively. Under these conditions, the number density is 1.81×10^{22} m^{-3}, the mean free path is 0.091 mm, and the Knudsen number is estimated to be 0.016. The computational region is divided into 40×20 sampling cells, each of which is divided into a 5×5 collision cells so that the collision cell is smaller than the mean free path. Initially, each sampling and collision cell contains 400 and 16 particles, respectively. The time step is chosen to be 0.9 of the mean free time. A sampling is performed in every two simulation time steps and a flow field is obtained by an average of 100 samplings.

The temperature of the bottom wall is increased instantly at the time zero from the initial value to a specified value, which corresponds to the maximum Rayleigh number in our simulation condition. The temperature of the top wall is unchanged from the initial value. Under these boundary temperature conditions, the simulation is performed for more than 100 000 time steps. The temperature of the bottom wall is, then, decreased to a next specified value, and the simulation with a smaller Rayleigh number is performed. In this way, the temperature of the bottom wall is reduced stepwise, and simulations with a different Rayleigh number are performed.

The diffuse reflection boundary condition, in which a reflected particle has velocity components randomly sampled from the Maxwellian distribution corresponding to the surface temperature, is assumed at the top and bottom walls. The specular reflection boundary condition, in which the perpendicular velocity component of the incident particle is reversed and the tangential velocity component is unchanged, is assumed at the side walls. The gravitational acceleration is chosen to be a hypothetical value so that the average increase of kinetic energy of a particle at the bottom wall is sufficient to bring it to the top of the system [3,5,6]: $g=(k_B\Delta T)/(mL_y)$, where g is the hypothetical gravity, k_B the Boltzmann constant, ΔT the temperature difference, m the particle mass, and L_y the distance between the top and bottom walls. The bottom wall temperature ranges from 120 to 400 K, and the corresponding Rayleigh numbers (Ra) are from 407 to 4527. The critical Rayleigh number (Ra_c) of this system is 1708, which is obtained from the linear stability analysis of the macroscopic hydrodynamic equations based on the Boussinesq approximation [15]. The wavelength at the critical Rayleigh number is 2.016, and thus the aspect ratio of the computational region is set equal to this value.

III. MACROSCOPIC FLOW FIELD

The absolute value of the flow velocity observed in the center of the computational region (V_{cent}) is shown in Fig. 1 as a function of time for Ra=1870. The velocity is normalized by the reference velocity (V_{ref}), which is defined as the most probable molecular thermal speed for the average temperature in the system. After the initial transient, the flow velocity is shown to fluctuate around an average value.

In this case, the vertical diffusion time defined as $t_v=L_y^2/\kappa$, where κ is the thermal diffusivity, is estimated to be about 2300 time steps from the Chapman-Enskog theory [16]. The simulation is thus performed for more than 50 times of the vertical diffusion time. In our simulation conditions, Ra=1870 is the closest to the hydrodynamical critical value of $Ra_c=1708$. The parameter which shows the difference between the simulation condition and the hydrodynamical critical value, $\epsilon=(Ra-Ra_c)/Ra_c$, is 0.095. Although the fluctuations were always found in Fig. 1, a large transient was not observed except for the initial transient. This is also found in a temperature history, and is always seen in other cases of our simulations. The small aspect ratio of the computational region and the side wall boundary conditions may be responsible for it.

The maximum velocity in the system (V_{max}) is shown in Fig. 2 against the parameter ϵ. The data points show a long-time average after the initial transient (between 20 000 and 120 000 time steps in this case), and the error bars indicate the range of data distributions.

Some typical examples of velocity vectors and isothermal contours, which are obtained by averaging the flow fields between 80 000 and 85 000 time steps, are shown in Fig. 3. The scaling factor of velocity vectors for $\epsilon=-0.448$, -0.118, and 0.095 are five times larger

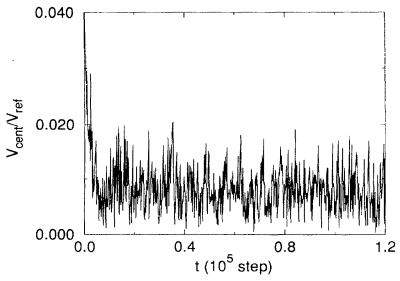

FIG. 1. The absolute value of the flow velocity at the center of computational region (V_{cent}) as a function of time for Ra=1870. The velocity is normalized by the reference velocity (V_{ref}) defined as the most probable molecular thermal speed for the average temperature in the system.

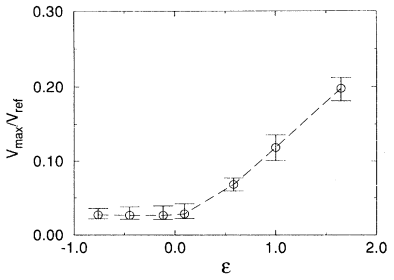

FIG. 2. The maximum velocity in the system (V_{max}) vs the parameter $\epsilon=(\mathrm{Ra}-\mathrm{Ra}_c)/\mathrm{Ra}_c$, where the critical Rayleigh number (Ra_c) is obtained from the linear stability analysis. The data points (○) show a long-time average after the initial transient, and the error bars indicate the range of data distributions.

than that for $\epsilon=0.583$.

It is found in Figs. 2 and 3 that the flow velocity is small, and that no convection rolls appear when ϵ is smaller than zero, though local flows are seen somewhere in the system. The temperature fields show the heat conduction states with a linear temperature variation in the vertical direction. Although the flow fields shown in Fig. 3 are obtained at a particular time, similar flow fields showing the heat conduction state are always observed at different time steps for $\epsilon<0$.

The convection rolls appear and the temperature field is slightly affected for $\epsilon=0.095$. Similar roll-like flows are always observed at different time steps for $\epsilon=0.095$. Large and stable convection rolls are established for $\epsilon=0.583$. The convection state is thus found for $\epsilon>0$. As was reported in Ref. [7], the transition of temperature distributions between heat conduction and convection occurs at around the hydrodynamic critical Rayleigh number ($\epsilon=0$). The DSMC method performed here is thus confirmed to reproduce the transition.

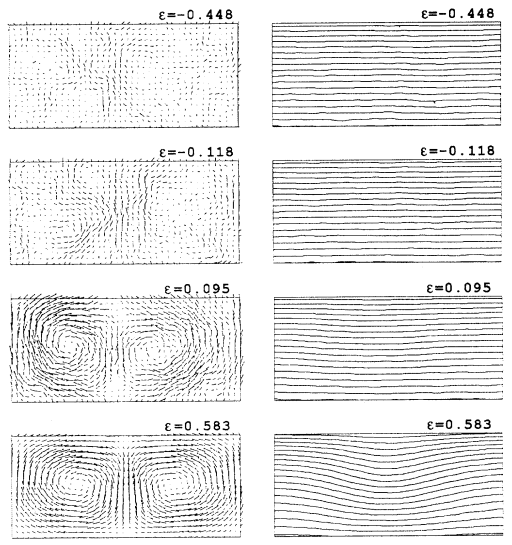

FIG. 3. Examples of velocity vectors (left) and isothermal contours (right) obtained by averaging the flow fields between 80 000 and 85 000 time steps. The scaling factor of velocity vectors for $\epsilon=-0.448$, -0.118, and 0.095 are five times larger than that for $\epsilon=0.583$.

IV. THERMODYNAMIC FLUCTUATIONS

In this section, correlations of temperature fluctuations are studied. Since the nonequilibrium constraints are imposed at the top and bottom walls in our system, the reduced correlation of temperature fluctuations is defined in the vertical direction (y) by averaging over horizontal direction (x) as

$$\langle \delta T(y,t)\delta T(y',t)\rangle=\frac{1}{L_x}\int_0^{L_x}\langle \delta T(x,y,t)\delta T(x,y',t)\rangle dx \ , \tag{1}$$

where δT is a temperature fluctuation which is a deviation from an average temperature, $\langle\ \rangle$ denotes a short-time average over 25 successive flow fields (5000 time steps), and L_x is the width of the computational region. The reduced correlation includes both equilibrium and nonequilibrium contributions and represents the relationship of temperature fluctuations between the elevation y and y'.

The correlation coefficient is then defined as

$$f(y,y',t)=\frac{\langle \delta T(y,t)\delta T(y',t)\rangle}{\langle \delta T(y',t)\delta T(y',t)\rangle} \ . \tag{2}$$

The correlation coefficient with one elevation fixed at $y'/L_y=0.725$ is shown in Fig. 4 for $\epsilon=0.095$ as an example. The correlation coefficient is seen to be long ranged with a peak of the autocorrelation ($y=y'$). It is shown that the degree of correlation decreases with increasing distance. The long-range correlation functions with a peak were already obtained in the heat conduction state without gravity [8,11,12].

In order to see the degree of correlation at a certain

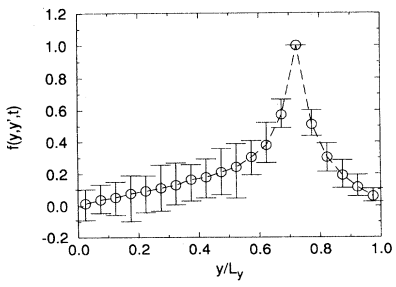

FIG. 4. The correlation coefficient $f(y,y',t)$ with one elevation fixed at $y'/L_y=0.725$ as a function of elevation for $\epsilon=0.095$, where L_y is the height of the computational region. The data points (○) show a long-time average after the initial transient, and the error bars indicate the range of data distributions.

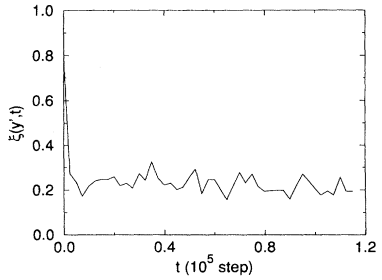

FIG. 5. The characteristic length $\xi(y',t)$ at $y'/L_y=0.725$ as a function of time for $\epsilon=0.095$.

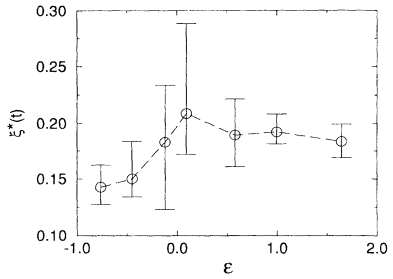

FIG. 7. The average characteristic length $\xi^*(t)$ in the system vs ϵ. The data points (○) show a long-time average after the initial transient, and the error bars indicate the range of data distributions.

elevation, the characteristic length is defined as

$$\xi(y',t)=\frac{1}{L_y}\int_0^{L_y} f(y,y',t)dy \ . \tag{3}$$

The characteristic length indicates a measure of the distance where the effect of the fluctuation spreads. The definition of the characteristic length given by Eq. (3) is similar to that of the integral scale, which is known as a characteristic scale of turbulence structure [17].

The characteristic length at $y'/L_y=0.725$ is shown in Fig. 5 as a function of time for $\epsilon=0.095$. After the initial transient, the characteristic length is shown to fluctuate around an average value, and no large transient is observed. This is also seen at different elevations and in other cases of our simulations.

The characteristic length for different values of ϵ is shown in Fig. 6 as a function of elevation. In the conduction state with a large negative value of ϵ ($\epsilon=-0.448$), the characteristic length is almost uniform in the system except for the region close to the top and bottom walls. In the convection state with a large positive value of ϵ ($\epsilon=0.583$), however, the characteristic length is longer at high elevation around $y=0.7$ and shorter at low elevation around $y=0.3$. In the cases with a relatively small value of ϵ ($\epsilon=-0.118$ and 0.095), the characteristic length is slightly longer at higher elevation. It is thus found in terms of the characteristic length that the feature of the convection state is seen in the small-ϵ cases, even if $\epsilon<0$.

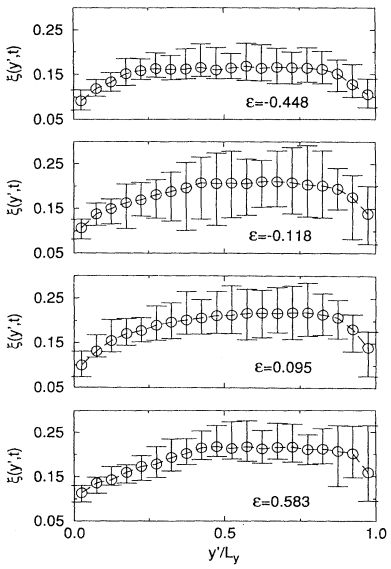

FIG. 6. The dependence of characteristic length $\xi(y',t)$ on elevation y' for different values of ϵ. The data points (○) show a long-time average after the initial transient, and the error bars indicate the range of data distributions.

In order to see the dependence of the characteristic length on ϵ, the average characteristic length in the system is defined as

$$\xi^*(t)=\frac{1}{L_y}\int_0^{L_y}\xi(y',t)dy' \ , \tag{4}$$

and shown in Fig. 7. The average characteristic length is shown to be shorter for the conduction state with large negative ϵ ($\epsilon=-0.448$) than for the convection state with large positive ϵ ($\epsilon=0.583$). In the cases with small ϵ close to zero ($\epsilon=-0.118$ and 0.095), the average characteristic length is longer than that in these two states. The data distributions are also larger for $\epsilon=-0.118$ and 0.095 than for $\epsilon=-0.448$ and 0.583. It is thus found at around the critical Rayleigh number ($\epsilon=0$) that the average distance where the effect of the fluctuation spreads is elongated and the degree of correlation is relatively high.

V. SUMMARY

In this study, the instability in the RB conduction-convection system has been simulated using the DSMC method.

In the conduction state with large negative ϵ, the characteristic length, which indicates a measure of the distance where the effect of the fluctuation spreads, is almost uniform spatially in the system. In the convection state with large positive ϵ, however, the characteristic length is relatively long at high elevation, and this feature is seen in the state with negative ϵ close to zero. The

average characteristic length in the system was shown to be elongated and the long-range correlations of temperature fluctuations are found to grow in the transition at around $\epsilon=0$.

Our results indicate that the correlations of fluctuations play an important roll in the flow instability, and the DSMC method is shown to be valuable tool for studying the macroscopic flow transitions.

[1] See, for instance (recently), R. E. Ecke, R. Mainieri, and T. S. Sullivan, Phys. Rev. A **44**, 8103 (1991); G. Ahlers, Physica D **51**, 421 (1991); Y. C. Michel and K. T. Young, Trans. ASME J. Heat Transfer **114**, 622 (1992); C. W. Meyer, D. S. Cannell, and G. Ahlers, Phys. Rev. A **45**, 8583 (1992); Y. Hu, R. Ecke, and G. Ahlers, Phys. Rev. E **48**, 4399 (1992); S. W. Morris, E. Bodenschatz, D. S. Cannell, and G. Ahlers, Phys. Rev. Lett. **71**, 2026 (1993); for a review of pattern formation, see M. C. Cross and P. C. Hohenberg, Rev. Mod. Phys. **65**, 851 (1993).

[2] See, for instance (recently), D. Mukutmoni and K. T. Yang, Trans. ASME J. Heat Transfer **115**, 360 (1993); H. Xi and J. D. Gunton, Phys. Rev. E **47**, R2987 (1993); F. Stella, G. Guj, and E. Leonardi, J. Fluid Mech. **254**, 375 (1993); W. Decker, W. Pesch, and A. Weber, Phys. Rev. Lett. **73**, 648 (1994); see also M. C. Cross and P. C. Hohenberg, in Ref. [1].

[3] M. Mareschal and E. Kestemont, J. Stat. Phys. **48**, 1187 (1987); D. C. Rapaport, Phys. Rev. Lett. **60**, 2480 (1988).

[4] M. Mareschal, M. M. Mansour, A. Puhl, and E. Kestemont, Phys. Rev. Lett. **61**, 2550 (1988); A. Puhl, M. M. Mansour and M. Mareschal, Phys. Rev. A **40**, 1999 (1989); J. A. Given and E. Clementi, J. Chem. Phys. **90**, 7376 (1989).

[5] A. L. Garcia, in *Microscopic Simulations of Complex Flows,* edited by M. Mareschal (Plenum, New York, 1990), p. 177; S. Stefanov and C. Cercignani, Eur. J. Mech. B **11**, 543 (1992).

[6] A. Garcia and C. Penland, J. Stat. Phys. **64**, 1121 (1991); F. Baras, M. M. Mansour, and A. L. Garcia, Phys. Rev. E **49**, 3512 (1994).

[7] T. Watanabe, H. Kaburaki, and M. Yokokawa, Phys. Rev. E **49**, 4060 (1994).

[8] G. Nicolis and M. M. Mansour, Phys. Rev. A **29**, 2845 (1984).

[9] M. Mareschal and E. Kestemont, Phys. Rev. A **30**, 1158 (1984).

[10] A. L. Garcia, Phys. Rev. A **34**, 1454 (1986); Phys. Lett. A **119**, 379 (1987).

[11] A. L. Garcia, M. M. Mansour, G. C. Lie, and E. Clementi, J. Stat. Phys. **47**, 209 (1987).

[12] M. M. Mansour, A. L. Garcia, G. C. Lie, and E. Clementi, Phys. Rev. Lett. **58**, 874 (1987).

[13] I. Rehberg, S. Rasenat, M. de la Torre Juárez, W. Schöpf, F. Hörner, G. Ahlers, and H. R. Brand, Phys. Rev. Lett. **67**, 596 (1991).

[14] G. A. Bird, *Molecular Gas Dynamics* (Clarendon, Oxford, 1976).

[15] S. Chandrasekhar, *Hydrodynamic and Hydromagnetic Stability* (Clarendon, Oxford, 1961).

[16] S. Chapman and T. G. Cowling, *The Mathematical Theory of Non-Uniform Gases* (Cambridge University Press, Cambridge, 1970).

[17] J. O. Hinze, *Turbulence* (McGraw-Hill, New York, 1975).